

Tensor-based Multimodal Learning for Prediction of Pulmonary Arterial Wedge Pressure from Cardiac MRI

Prasun C. Tripathi^{1*}, Mohammad N. I. Suvon¹, Lawrence Schobs¹, Shuo Zhou¹, Samer Alabed^{2,3,4}, Andrew J. Swift^{2,3,4}, and Haiping Lu^{1,3}

¹ Department of Computer Science, The University of Sheffield, Sheffield, United Kingdom

² Department of Infection, Immunity and Cardiovascular Disease, The University of Sheffield, Sheffield, United Kingdom

³ INSIGNEO, Institute for in Silico Medicine, The University of Sheffield, Sheffield, United Kingdom

⁴ Department of Clinical Radiology, Sheffield Teaching Hospitals, Sheffield, United Kingdom

{*p.c.tripathi, mnisuvon1, laschobs1, shuo.zhou, s.alabed, a.j.swift, h.lu}@sheffield.ac.uk

Abstract. Heart failure is a serious and life-threatening condition that can lead to elevated pressure in the left ventricle. Pulmonary Arterial Wedge Pressure (PAWP) is an important surrogate marker indicating high pressure in the left ventricle. PAWP is determined by Right Heart Catheterization (RHC) but it is an invasive procedure. A non-invasive method is useful in quickly identifying high-risk patients from a large population. In this work, we develop a tensor learning-based pipeline for identifying PAWP from multimodal cardiac Magnetic Resonance Imaging (MRI). This pipeline extracts spatial and temporal features from high-dimensional scans. For quality control, we incorporate an epistemic uncertainty-based binning strategy to identify poor-quality training samples. To improve the performance, we learn complementary information by integrating features from multimodal data: cardiac MRI with short-axis and four-chamber views, and Electronic Health Records. The experimental analysis on a large cohort of 1346 subjects who underwent the RHC procedure for PAWP estimation indicates that the proposed pipeline has a diagnostic value and can produce promising performance with significant improvement over the baseline in clinical practice (i.e., $\Delta\text{AUC} = 0.10$, $\Delta\text{Accuracy} = 0.06$, and $\Delta\text{MCC} = 0.39$). The decision curve analysis further confirms the clinical utility of our method.

Keywords: Cardiac MRI · Multimodal Learning · Pulmonary Arterial Wedge Pressure.

1 Introduction

Heart failure is usually characterized by the inability of the heart to supply enough oxygen and blood to other organs of the body [5]. It is a major cause of

mortality and hospitalization [16]. Elevated Pulmonary Arterial Wedge Pressure (PAWP) is indicative of raised left ventricular filling pressure and reduced contractility of the heart. In the absence of mitral valve or pulmonary vasculature disease, PAWP correlates with the severity of heart failure and risk of hospitalization [2]. While PAWP can be measured by invasive and expensive Right Heart Catheterization (RHC), simpler and non-invasive techniques could aid in better monitoring of heart failure patients.

Cardiac Magnetic Resonance Imaging (MRI) is an effective tool for identifying various heart conditions and its ability to detect disease and predict outcome has been further improved by machine learning techniques [4]. For instance, Swift et al. [20] introduced a machine-learning pipeline for identifying Pulmonary Artery Hypertension (PAH). Goh et al. [7] performed right ventricular remodeling for predicting treatment failure in heart patients using cardiac MRI. Recently, Uthoff et al. [21] developed geodesically smoothed tensor features for predicting mortality in PAH.

Cardiac MRI scans contain high-dimensional spatial and temporal features generated throughout the cardiac cycle. The small number of samples compared to the high-dimensional features poses a challenge for machine learning classifiers. To address this issue, Multilinear Principal Component Analysis (MPCA) [13] utilizes a tensor-based approach to reduce feature dimensions while preserving the information for each mode, i.e. spatial and temporal information in cardiac MRI. Hence, the MPCA method is well-suited for analyzing cardiac MRI scans. The application of the MPCA method to predict PAWP might further increase the diagnostic yield of cardiac MRI in heart failure patients and help to establish cardiac MRI as a non-invasive alternative to RHC. Existing MPCA-based pipelines for cardiac MRI [20,21,3] rely on manually labeled landmarks that are used for aligning heart regions in cardiac MRI. The manual labeling of landmarks is a cumbersome task for physicians and impractical for analyzing large cohorts. Moreover, even small deviations in the landmark placement may significantly impact the classification performance of automatic pipelines [18]. To tackle this challenge, we leverage automated landmarks with uncertainty quantification [17] in our pipeline.

In recent years, multimodal learning obtained remarkable performance for solving various healthcare problems [1]. The utilization of EHR (Electronic Health Record) features enhanced the diagnostic power in several studies [19]. This motivates us to extract complementary information from multimodal data from short-axis, four-chamber, and EHR features. Specifically, we aim to utilize EHR features identified in the baseline work by Garg et al. [6] for PAWP prediction. These features include left arterial volume and left ventricular mass.

Our **main contributions** are summarized as follows: 1) **Methodology:** We developed a fully automatic pipeline for PAWP prediction using cardiac MRI and EHR data, which includes automatic landmark detection with uncertainty quantification, an uncertainty-based binning strategy for training sample selection, tensor feature learning, and multimodal feature integration. 2) **Effectiveness:** Extensive experiments on the cardiac MRI scans of 1346 patients with various

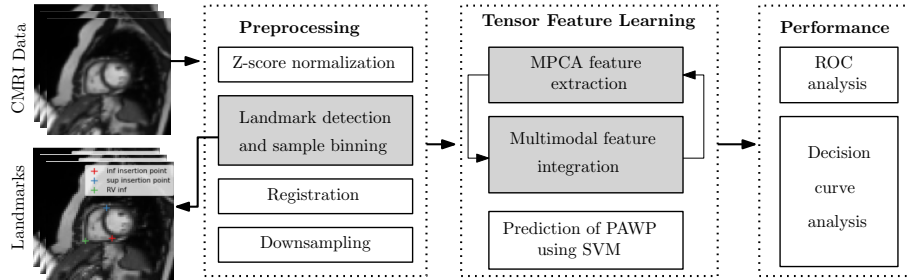


Fig. 1: The schematic overview of the PAWP prediction pipeline including pre-processing, tensor feature learning, and performance analysis. The blocks in gray color are explained in more detail in Section 2.

heart diseases validated our pipeline with a significant improvement ($\Delta\text{AUC} = 0.1027$, $\Delta\text{Accuracy} = 0.0628$, and $\Delta\text{MCC} = 0.3917$) over the current clinical baseline. 3) **Clinical utility:** Decision curve analysis indicates the diagnostic value of our pipeline, which can be used in screening high-risk patients from a large population.

2 Methods

As shown in Fig. 1, the proposed pipeline for PAWP prediction comprises three components: preprocessing, tensor feature learning, and performance analysis.

Cardiac MRI Preprocessing: The preprocessing of cardiac MRI contains (1) normalization of scans, (2) automatic landmark detection, (3) inter-subject registration, and (4) in-plane downsampling. We standardize cardiac MRI intensity levels using Z-score normalization [9] to eliminate inter-subject variations. Furthermore, we detect automated landmarks, which is explained in the next paragraph. We perform affine registration to align the heart regions of different subjects to a target image space. We then carry out in-plane scaling of scans by max-pooling at 2, 4, 8, and 16 times and obtain down-sampled resolutions of 128×128 , 64×64 , 32×32 , and 16×16 , respectively.

Landmark Detection and Uncertainty-based Sample Binning: We utilize supervised learning to automate landmark detection using an ensemble of Convolutional Neural Networks (CNNs) for each modality (short-axis and four-chamber). We use the U-Net-like architecture and utilize the same training regime implemented in [17]. We employ *Ensemble Maximum Heatmap Activation (E-MHA)* strategy [17] which incorporates an ensemble of 5 models for each modality. We utilize three landmarks for each modality, with the short-axis modality using the inferior hinge point, superior hinge point, and inferolateral inflection point of the right ventricular apex, and the four-chamber modality using the left ventricular apex and mitral and tricuspid annulus. E-MHA produces

an associated uncertainty estimate for each landmark prediction, representing the model’s epistemic uncertainty as a continuous scalar value.

A minor error in landmark prediction can result in incorrect image registration [18]. To address this issue, we hypothesize that incorrectly preprocessed samples resulting from inaccurate landmarks can introduce ambiguity during model training. For quality control, it is crucial to identify and effectively handle such samples. In this study, we leverage predicted landmarks and epistemic uncertainties to tackle this problem using uncertainty-based binning. To this end, we partition the training scans based on the uncertainty values of the landmarks. The predicted landmarks are divided into K quantiles, i.e., $Q = \{q_1, q_2, \dots, q_K\}$, based on the epistemic uncertainty values. We then iteratively filter out training samples starting from the highest uncertain quantile. A sample is discarded if the uncertainty of any of its landmarks lies in quantile q_k where $k = \{1, 2, \dots, K\}$. The samples are discarded iteratively until there is no improvement in the validation performance, as measured by the area under the curve (AUC), for two subsequent iterations.

Tensor Feature Learning: To extract features from processed cardiac scans, we employ tensor feature learning, i.e. Multilinear Principal Component Analysis (MPCA) [13], which learns multilinear bases from cardiac MRI stacks to obtain low-dimensional features for prediction. Suppose we have M scans as third-order tensors in the form of $\{\mathcal{X}_1, \mathcal{X}_2, \dots, \mathcal{X}_M \in \mathbb{R}^{I_1 \times I_2 \times I_3}\}$. The low-dimensional tensor features $\{\mathcal{Y}_1, \mathcal{Y}_2, \dots, \mathcal{Y}_M \in \mathbb{R}^{P_1 \times P_2 \times P_3}\}$ are extracted by learning three ($N = 3$) projection matrices $\{U^{(n)} \in \mathbb{R}^{I_n \times P_n}, n = 1, 2, 3\}$ as follows:

$$\mathcal{Y}_m = \mathcal{X}_m \times_1 U^{(1)T} \times_2 U^{(2)T} \times_3 U^{(3)T}, m = 1, 2, \dots, M, \quad (1)$$

where $P_n < I_n$, and \times_n denotes a mode-wise product. Therefore, the feature dimensions are reduced from $I_1 \times I_2 \times I_3$ to $P_1 \times P_2 \times P_3$. We optimize the projection matrices $\{U^{(n)}\}$ by maximizing total scatter $\psi_{\mathcal{Y}} = \sum_{m=1}^M \|\mathcal{Y}_m - \bar{\mathcal{Y}}\|_F^2$, where $\bar{\mathcal{Y}} = \frac{1}{M} \sum_{m=1}^M \mathcal{Y}_m$ is the mean tensor feature and $\|\cdot\|_F$ is the Frobenius norm [12]. We solve this problem using an iterative projection method. In MPCA, $\{P_1, P_2, P_3\}$ can be determined by the explained variance ratio, which is a hyperparameter. Furthermore, we apply Fisher discriminant analysis to select the most significant features based on their Fisher score [10]. We select the top k -ranked features and employ Support Vector Machine (SVM) for classification.

Multimodal Feature Integration: To enhance performance, we perform multimodal feature integration using features extracted from the short-axis, four-chamber, and EHR. We adopt two strategies for feature integration, namely the early and late fusion of features [8]. In early fusion, the features are fused at the input level without doing any transformation. We concatenate features from the short-axis and four-chamber to perform this fusion. We then apply MPCA [13] on the concatenated tensor, enabling the selection of multimodal features. In late fusion, the integration of features is performed at the common latent space that allows the fusion of features that have different dimensionalities. In this way,

Table 1: Baseline characteristics of included patients. p values were obtained using t -test [23].

	Low PAWP(≤ 15)	High PAWP(> 15)	p -value
Number of patients	940	406	-
Age (in years)	64.8 ± 14.2	70.5 ± 10.6	< 0.01
Body Surface Area (BSA)	1.88 ± 0.28	1.93 ± 0.24	< 0.01
Heart Rate (bpm)	73.9 ± 15.5	67.6 ± 15.9	< 0.01
Left Ventricle Mass (LVM)	92.3 ± 25	106 ± 33.1	< 0.01
Left Atrial Volume (ml^2)	72.2 ± 33.7	132.2 ± 56.7	< 0.01
PAWP (mmHg)	10.3 ± 3.1	21.7 ± 4.96	< 0.01

we can perform a late fusion of EHR features with short-axis and four-chamber features. However, we can not perform an early fusion of EHR features with short-axis and four-chamber features.

Performance Evaluation: In this paper, we use three primary metrics: Area Under Curve (AUC), accuracy, and Matthew’s Correlation Coefficient (MCC), to evaluate the performance of the proposed pipeline. Decision Curve Analysis (DCA) is also conducted to demonstrate the clinical utility of our methodology.

3 Experimental Results and Analysis

Study Population: Patients with suspected pulmonary hypertension were identified after institutional review board approval and ethics committee review. A total of 1346 patients who underwent Right Heart Catheterization (RHC) and cardiac MRI scans within 24 hours were included. Of these patients, 940 had normal PAWP (≤ 15 mmHg), while 406 had elevated PAWP (> 15 mmHg). Table 1 summarizes baseline patient characteristics. RHC was performed using a balloon-tipped 7.5 French thermodilution catheter.

Cardiac MRI data: MRI scans were obtained using a 1.5 Tesla whole-body GE HDx MRI scanner (GE Healthcare, Milwaukee, USA) equipped with 8-channel cardiac coils and retrospective electrocardiogram gating. Two cardiac MRI protocols, short-axis and four-chamber, were employed, following standard clinical protocols to acquire cardiac-gated multi-slice steady-state sequences with a slice thickness of 8 mm, a field of view of 48×43.2 , a matrix size of 512×512 , a bandwidth of 125 kHz, and TR/TE of 3.7/1.6 ms. The proposed method works on volumetric slices of cardiac MRI containing 20 temporal phases.

Experimental Design: We conducted experiments on short-axis and four-chamber scans across four scales. To determine the optimal parameters, we performed 10-fold cross-validation on the training set. From MPCA, we selected the top 210 features. We employed early and late fusion on Short-axis and Four-chamber scans, respectively, while EHR features were only fused using the late fusion strategy. We divided the data into a training set of 1081 cases and a testing set of 265 cases. To simulate a real testing scenario, we designed the

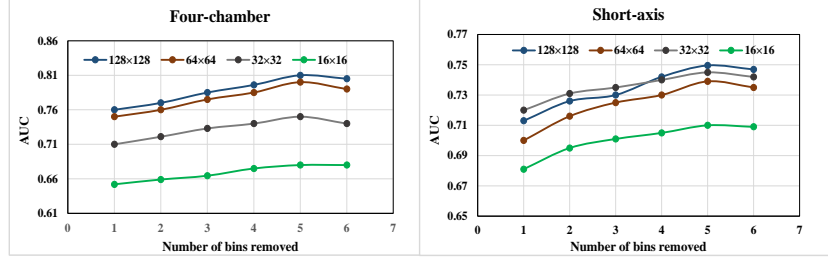


Fig. 2: Performance comparison of removing a different number of bins of training data on 10-fold cross-validation.

Table 2: Performance comparison using three metrics (with **best** in bold and second best underlined). FC: Four-Chamber features; SA: Short-Axis features; EHR: Electronic Health Record features. The standard deviations of methods were obtained by dividing the test set into 5 parts based on the diagnosis time.

Modality	Resolution	AUC	Accuracy	MCC
Unimodal (EHR) [6]	-	0.7300 ± 0.04	0.7400 ± 0.03	0.1182 ± 0.03
Unimodal (SA)	64×64	0.7391 ± 0.05	0.7312 ± 0.07	0.3604 ± 0.02
	128×128	0.7495 ± 0.05	0.7321 ± 0.04	0.3277 ± 0.01
Unimodal (FC)	64×64	0.8034 ± 0.02	0.7509 ± 0.04	0.4240 ± 0.02
	128×128	0.8100 ± 0.04	0.7925 ± 0.05	0.4666 ± 0.02
Bi-modal (SA and FC): Early fusion	64×64	0.7998 ± 0.01	0.7698 ± 0.03	0.4185 ± 0.03
	128×128	0.7470 ± 0.02	0.7283 ± 0.02	0.3512 ± 0.02
Bi-modal (SA and FC): Late fusion	64×64	0.8028 ± 0.04	0.7509 ± 0.03	0.3644 ± 0.01
	128×128	0.8122 ± 0.03	0.7547 ± 0.03	0.3594 ± 0.02
Bi-modal (SA and EHR): Late fusion	64×64	0.7564 ± 0.04	0.7585 ± 0.02	0.3825 ± 0.02
	128×128	0.7629 ± 0.03	0.7434 ± 0.03	0.3666 ± 0.03
Bi-modal (FC and EHR): Late fusion	64×64	0.8061 ± 0.03	0.7709 ± 0.02	0.4435 ± 0.02
	128×128	0.8135 ± 0.02	0.7925 ± 0.02	0.4999 ± 0.03
Tri-modal (FC, SA, and EHR)	64×64	0.8146 ± 0.04	0.7774 ± 0.03	0.4460 ± 0.02
Hybrid fusion	128×128	0.8327 ± 0.06	0.8038 ± 0.05	0.5099 ± 0.04

experiments such that patients diagnosed in the early years were part of the training set, while patients diagnosed in recent years were part of the testing set. We also partitioned the test into 5 parts based on the diagnosis time to perform different runs of methods and report standard deviations of methods in comparison results. For SVM, we selected the optimal hyper-parameters from $\{0.001, 0.01, 0.1, 1\}$ using grid search technique. The code for the experiments has been implemented in Python (version 3.9). We leveraged the cardiac MRI preprocessing pipeline and MPCA from the Python library PyKale [11] and SVM implementation is taken from scikit-learn [14].

Uncertainty-Based Sample Binning: To improve the quality of training data, we used quantile binning to remove training samples with uncertain landmarks. The landmarks were divided into 50 bins, and then removed one bin at a

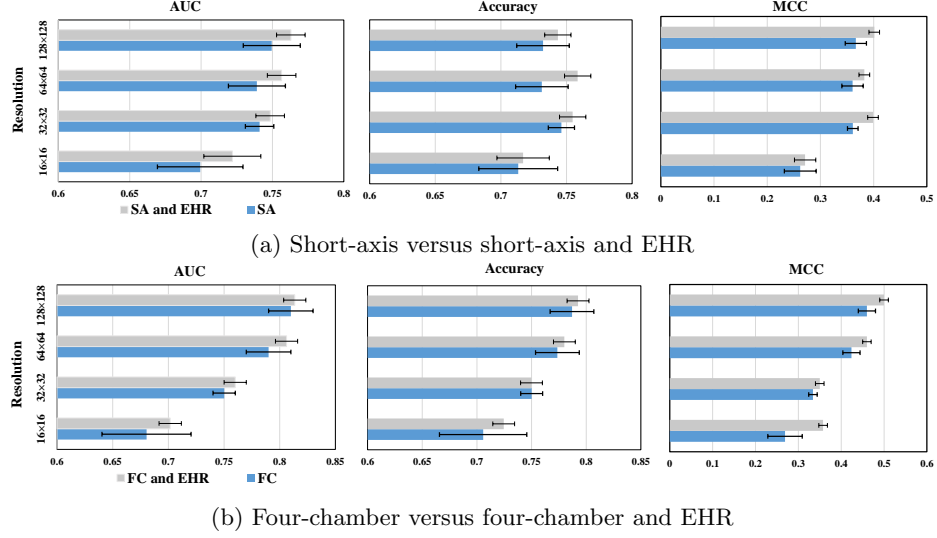


Fig. 3: The effect of combining EHR features on short-axis and four-chamber. SA: Short-axis; FC: Four-chamber.

time in the descending order of their uncertainties. Figure 2 depicts the results of binning using 10-fold cross-validation on the training set, where the performance improves consistently over the four scales when removed bins ≤ 5 . Based on the results, we removed 5 bins (129 out of 1081 samples) from the training set, and used the remaining 952 training samples for the following experiments.

Unimodal Study: We compared the performance of single modalities including short-axis, four-chamber, and EHR features in this experiment. As a baseline, we used previously reported EHR features [6], which include left ventricle mass and left arterial volume. Table 2 presents the performance of the unimodal models. It is observed that the four-chamber modality model produced a better performance with improvement over the baseline ($\Delta\text{AUC} = 0.0800$ $\Delta\text{Accuracy} = 0.0527$ and $\Delta\text{MCC} = 0.3484$). This experiment indicates that tensor-based features have a diagnostic value.

Bi-modal Study: In this experiment, we compared the performance of bi-modal models. As shown in Table 2, bimodal (four-chamber and EHR) produces superior performance (i.e., $\text{AUC} = 0.8135$, $\text{Accuracy} = 0.7925$ and $\text{MCC} = 0.4999$) among bi-modal models. Next, we investigated the effect of fusing EHR features with short-axis and four-chamber modalities in Fig. 3. It can be observed from these figures that the fusion of EHR features enhances the diagnostic power of cardiac MRI modalities at all scales. The bi-modal (four-chamber and EHR) model achieved the improvement in the performance ($\Delta\text{AUC} = 0.0035$ and $\Delta\text{MCC} = 0.0333$) over the unimodal (four-chamber) model.

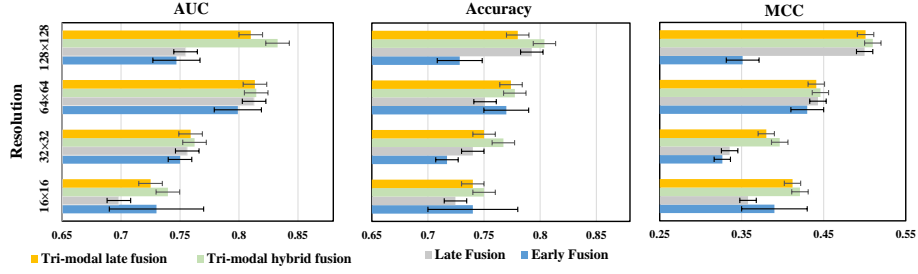


Fig. 4: The effect of combining EHR features on the bi-modals including early and late fusion of four-chamber and short-axis. Early fusion: early fusion of short-axis and four-chamber; late fusion: late fusion of short-axis and four-chamber.

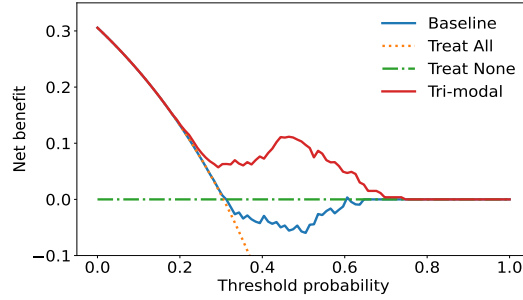


Fig. 5: Evaluating clinical utility of our method using Decision Curve Analysis (DCA) [22]. “Treat All” means treating all patients, regardless of their actual disease status, while “Treat None” means treating no patients at all. Our predictive model’s net benefit is compared with the net benefit of treating everyone or no one to determine its overall utility.

Effectiveness of Tri-modal: In this experiment, we performed a fusion of EHR features with the bi-modal models to create two tri-modal models. The first tri-modal is tri-modal late (EHR with a late fusion of short-axis and four-chamber) and the second tri-modal is a tri-modal hybrid (EHR with an early fusion of short-axis and four-chamber). As shown in Fig. 4, EHR features enhance the performance of bi-modal models and tri-modal hybrid outperforms all. The tri-modal hybrid achieved the best performance (i.e., $AUC = 0.8327$, $Accuracy = 0.8038$, and $MCC = 0.5099$) (see Table 2). This model obtained significant improvements over the baseline method (i.e., $\Delta AUC = 0.1027$, $\Delta Accuracy = 0.0628$, and $\Delta MCC = 0.3917$).

Decision Curve Analysis: We performed Decision Curve Analysis (DCA) [22,15] to show the potential clinical utility of the proposed method. As shown in Fig. 5, the Tri-modal model outperformed the baseline method for most possible benefit/harm preferences, where benefit indicates a positive net benefit (i.e. correct

diagnosis) and harm indicates a negative net benefit (i.e. incorrect diagnosis). The tri-modal model (the best model) obtained a higher net benefit between decision threshold probabilities of 0.30 and 0.70 which implies that our method has a diagnostic value and can be used in screening high-risk patients from a large population.

4 Conclusions

This paper proposed a tensor learning-based pipeline for PAWP classification. We demonstrated that: 1) tensor-based features have a diagnostic value for PAWP, 2) the integration of EHR features improved the performance of uni-modal and bi-modal methods, 3) the pipeline can be used to screen a large population, as shown using decision curve analysis. However, the current study is limited to single institutional data. In the future, we would like to explore the applicability of the method for multi-institutional data using domain adaptation techniques.

Acknowledgment

The study was supported by the Wellcome Trust grants 215799/Z/19/Z and 205188/Z/16/Z.

References

1. Acosta, J.N., Falcone, G.J., Rajpurkar, P., Topol, E.J.: Multimodal biomedical ai. *Nature Medicine* **28**(9), 1773–1784 (2022)
2. Adamson, P.B., Abraham, W.T., Bourge, R.C., Costanzo, M.R., Hasan, A., Yadav, C., Henderson, J., Cowart, P., Stevenson, L.W.: Wireless pulmonary artery pressure monitoring guides management to reduce decompensation in heart failure with preserved ejection fraction. *Circulation: Heart Failure* **7**(6), 935–944 (2014)
3. Alabed, S., Uthoff, J., Zhou, S., Garg, P., Dwivedi, K., Alandejani, F., Gosling, R., Schobs, L., Brook, M., Shahin, Y., et al.: Machine learning cardiac-mri features predict mortality in newly diagnosed pulmonary arterial hypertension. *European Heart Journal-Digital Health* **3**(2), 265–275 (2022)
4. Assadi, H., Alabed, S., Maiter, A., Salehi, M., Li, R., Ripley, D.P., Van der Geest, R.J., Zhong, Y., Zhong, L., Swift, A.J., et al.: The role of artificial intelligence in predicting outcomes by cardiovascular magnetic resonance: a comprehensive systematic review. *Medicina* **58**(8), 1087 (2022)
5. Emdin, M., Vittorini, S., Passino, C., Clerico, A.: Old and new biomarkers of heart failure. *European Journal of Heart Failure* **11**(4), 331–335 (2009)
6. Garg, P., Gosling, R., Swoboda, P., Jones, R., Rothman, A., Wild, J.M., Kiely, D.G., Condliffe, R., Alabed, S., Swift, A.J.: Cardiac magnetic resonance identifies raised left ventricular filling pressure: prognostic implications. *European Heart Journal* **43**(26), 2511–2522 (2022)

7. Goh, Z., Balasubramanian, N., Alabed, S., Dwivedi, K., Shahin, Y., Rothman, A.M., Garg, P., Lawrie, A., Capener, D., Thompson, A., et al.: Cmr assessed maladaptive right ventricular remodelling predicts treatment failure in pulmonary arterial hypertension (2022)
8. Huang, S.C., Pareek, A., Zamanian, R., Banerjee, I., Lungren, M.P.: Multimodal fusion with deep neural networks for leveraging ct imaging and electronic health record: a case-study in pulmonary embolism detection. *Scientific reports* **10**(1), 1–9 (2020)
9. Jain, A., Nandakumar, K., Ross, A.: Score normalization in multimodal biometric systems. *Pattern recognition* **38**(12), 2270–2285 (2005)
10. Li, J., Cheng, K., Wang, S., Morstatter, F., Trevino, R.P., Tang, J., Liu, H.: Feature selection: A data perspective. *ACM Computing Surveys (CSUR)* **50**(6), 94 (2018)
11. Lu, H., Liu, X., Zhou, S., Turner, R., Bai, P., Koot, R.E., Chasmai, M., Schobs, L., Xu, H.: Pykale: Knowledge-aware machine learning from multiple sources in python. In: *Proceedings of the 31st ACM International Conference on Information & Knowledge Management*. pp. 4274–4278 (2022)
12. Lu, H., Plataniotis, K.N., Venetsanopoulos, A.: *Multilinear subspace learning: dimensionality reduction of multidimensional data*. CRC press (2013)
13. Lu, H., Plataniotis, K.N., Venetsanopoulos, A.N.: MPCA: Multilinear principal component analysis of tensor objects. *IEEE Transactions on Neural Networks* **19**(1), 18–39 (2008)
14. Pedregosa, F., Varoquaux, G., Gramfort, A., Michel, V., Thirion, B., Grisel, O., Blondel, M., Prettenhofer, P., Weiss, R., Dubourg, V., Vanderplas, J., Passos, A., Cournapeau, D., Brucher, M., Perrot, M., Duchesnay, E.: Scikit-learn: Machine learning in Python. *Journal of Machine Learning Research* **12**, 2825–2830 (2011)
15. Sadatsafavi, M., Adibi, A., Puhan, M., Gershon, A., Aaron, S.D., Sin, D.D.: Moving beyond auc: decision curve analysis for quantifying net benefit of risk prediction models. *European Respiratory Journal* **58**(5) (2021)
16. Savarese, G., Becher, P.M., Lund, L.H., Seferovic, P., Rosano, G.M., Coats, A.J.: Global burden of heart failure: a comprehensive and updated review of epidemiology. *Cardiovascular research* **118**(17), 3272–3287 (2022)
17. Schöbs, L., Swift, A.J., Lu, H.: Uncertainty estimation for heatmap-based landmark localization. *IEEE Transactions on Medical Imaging* (2022)
18. Schobs, L., Zhou, S., Coglianò, M., Swift, A.J., Lu, H.: Confidence-quantifying landmark localisation for cardiac mri. In: *2021 IEEE 18th International Symposium on Biomedical Imaging (ISBI)*. pp. 985–988. IEEE (2021)
19. Suvon, M.N., Tripathi, P.C., Alabed, S., Swift, A.J., Lu, H.: Multimodal learning for predicting mortality in patients with pulmonary arterial hypertension. In: *2022 IEEE International Conference on Bioinformatics and Biomedicine (BIBM)*. pp. 2704–2710. IEEE (2022)
20. Swift, A.J., Lu, H., Uthoff, J., Garg, P., Coglianò, M., Taylor, J., Metherall, P., Zhou, S., Johns, C.S., Alabed, S., et al.: A machine learning cardiac magnetic resonance approach to extract disease features and automate pulmonary arterial hypertension diagnosis. *European Heart Journal-Cardiovascular Imaging* **22**(2), 236–245 (2021)
21. Uthoff, J., Alabed, S., Swift, A.J., Lu, H.: Geodesically smoothed tensor features for pulmonary hypertension prognosis using the heart and surrounding tissues. In: *Medical Image Computing and Computer Assisted Intervention–MICCAI 2020: 23rd International Conference, Lima, Peru, October 4–8, 2020, Proceedings, Part II* 23. pp. 253–262. Springer (2020)

22. Vickers, A.J., Elkin, E.B.: Decision curve analysis: a novel method for evaluating prediction models. *Medical Decision Making* **26**(6), 565–574 (2006)
23. Welch, B.L.: The generalization of ‘student’s’ problem when several different population variances are involved. *Biometrika* **34**(1-2), 28–35 (1947)